Micellar Solutions of Associative Triblock Copolymers: Entropic Attraction and Gas−Liquid Transition

Q. T. Pham[†] and W. B. Russel*

Department of Chemical Engineering, Princeton University, Princeton, New Jersey 08544

J. C. Thibeault and W. Lau

Research Laboratories, Rohm and Haas Company, Spring House, Pennsylvania 19477

Received December 28, 1998; Revised Manuscript Received March 3, 1999

ABSTRACT: We report the first clear observations of an entropy-driven phase transition between a dilute micellar "gas" and a disordered but highly associated micellar "liquid" realized with aqueous solutions of poly(ethylene oxide) chains fully end-capped with C_{16} and C_{18} hydrophobes. Dynamic light scattering and capillary viscometry determine the radii and aggregation numbers of the micelles and, together with the coexisting concentrations, permit estimates of the strength of the entropic attraction through the adhesive hard-sphere model. The behavior is qualitatively consistent with expectations for the entropy gain from the exchange of end blocks between cores of flowerlike micelles consisting of associative triblock copolymers.

1. Introduction

Water-soluble polymers with hydrophobic end blocks comprise a scientifically interesting and technologically successful class of hydrophobically modified associative polymers, primarily because of their ability to form highly viscous solutions with relatively simple viscoelastic behavior. This triblock, or telechelic, structure appeared as a commercial thickener more than a decade ago[1] and since has been the subject of numerous publications from academic and industrial groups. We defer to a recent review by Winnik and Yekta[2] for a detailed survey of this literature. The prototypical polymer of this family consists of a poly(ethylene oxide) (PEO) backbone of 8−100 kg/mol with C_{10}−C_{18} alkane terminal groups attached via urethane (isocyanate) coupling groups. Most attention has focused on intermediate molecular weights for the backbone, e.g. 35 kg/mol, and C_{12}−C_{16} hydrophobes, which impart highly viscous but tractable rheology in the absence of surfactants and cosolvents.

Research to date has established that such polymers in dilute solutions form micelles of radius R (∼20 nm) above a rather low critical micelle concentration ($c_{cmc} \ll 0.1$ wt %) that depends on the backbone molecular weight and the hydrophobe size.[3−8] The aggregation numbers are reported from 10 to 80, depending on the molecular structure and method of measurement. With increasing concentration the viscosity rises dramatically, well above that of comparable PEO solutions, providing convincing evidence of a high degree of association. The solutions generally exhibit an extended low shear plateau (to shear rates >100 s^{-1}) with a modest degree of shear thickening (less than a factor of 2), followed by rather dramatic shear thinning. The linear viscoelastic response is beautifully simple with a single relaxation time of 0.1−10 ms that varies exponentially with the size of the hydrophobe but only modestly with concentration, even with polydisperse backbones. Binary mixtures with the same backbone molecular weight but different hydrophobes display two distinct relaxation times. Although the dependence of the behavior on molecular structure, as well as surfactant and cosolvent concentration, is qualitatively clear, detailed comparisons are confounded by polydispersity of the backbone, incomplete capping with the hydrophobes, and (to a lesser extent) internal hydrophobes between PEO blocks. For example, one group reported a phase separation leading to coexistence between a highly viscous solution of fully end-capped chains and an equally concentrated but low-viscosity solution of unend-capped chains.[9]

Thus far the interpretation of the rheological behavior has depended on the reversible network theory,[10,11] effectively ignoring the observations of micelle formation at dilute concentrations. This approach succeeds qualitatively, since the shear viscosity is clearly controlled by dissociation of the hydrophobe from a junction or hydrophobic core. Capturing the concentration dependence, which derives from the high-frequency modulus for a fluid with a single relaxation time, is more difficult. Statistical analyses that modify the classical theory to allow for loops and junctions of modest and variable size can correlate the observations but overlook the physics of micellization and the rather large aggregation numbers detected.[12,13] Current theoretical developments for associative triblocks evolve from theories for interacting polymer brushes.[14−17] Instead of being adsorbed or grafted to a flat surface, the triblocks form flowerlike micelles with large aggregation number in a good solvent. Bridging between brushes or micelles gives rise to an entropic attraction; as concentration increases, the bridging density increases, approaching a limit similar to the transient network when a constant fraction of chains form bridges. The dissociation/association of the hydrophobe contributes to the interaction; however, as

[†] Current address Unilever Research, Edgewater, NJ.
* Corresponding author.

10.1021/ma982007v CCC: $18.00 © 1999 American Chemical Society
Published on Web 04/15/1999

Figure 1. Schematic of the Daoud−Cotton blob model for a micelle of radius R and outermost blob size ξ_o.

two micelles or brushes are compressed, excluded-volume interactions also play a significant role.

In this paper we report extensive characterization of such micellar solutions formed from narrow molecular weight PEO chains fully end-capped with C_{16} or C_{18} alkanes. These are the most ideal of systems examined to date and reveal some novel behavior that motivates a different interpretation of well-established features of the phenomena. First, the micellar solution exhibits a gas−liquid phase transition that is independent of temperature, as one would expect from the entropic attraction proposed in the flowerlike micelle model of Semenov et al.[14] Second, measurements of the low shear viscosity and diffusion coefficient for the dilute micellar phase establish the strength of the attraction as well as the size and aggregation number of the micelles. Third, the scaling and concentration dependence of the shear modulus resembles that of colloidal dispersions with soft repulsive potentials more than the expectations from either the Semenov et al. model or the reversible network theory. Consequently, we draw on the adhesive hard-sphere model together with the entropic attraction between micelles to interpret the behavior. Fourth, the relaxation time appears to scale with the diffusion time of the hydrophobe escaping the micelle, independent of the relaxation of the rest of the chain, providing the sole remaining link with the reversible network theory. Here we present the experimental findings and models for the micelles and phase behavior, leaving the viscoelasticity of the condensed liquid phase for the following paper.

2. Theories

2.1. Isolated Micelles. Recently Semenov et al.[14] treated solutions of flowerlike micelles, bypassing the thermodynamics of micellization by assuming a fixed aggregation number $p \gg 1$ and association energy $\chi \gg 1$. Then at dilute concentrations both hydrophobes must reside in the same micelle, resulting in a hydrophobic core and a corona of loops. The former is a melt of alkane chains, while the latter are highly stretched due to excluded-volume interactions among the segments of the hydrophilic midblock. The model of Daoud and Cotton[17] views the micelle as a series of radially growing, space-filling blobs (Figure 1) with size $\xi(r)$ that increases radially and is related to the number of arms ($2p$) by

$$4\pi r^2 = 2p\xi^2(r) \tag{1}$$

and the number of segments in the blob N_ξ by the Flory mean field theory.[18] For the flowerlike micelles, this approximation effectively snips each chain in half, ignoring the midpoint connection, and assumes the chains to be highly stretched due to the large aggregation numbers. In a good solvent, the root-mean-square end-to-end distance, s, depends on the excluded volume v/l^3, the segments per half-chain N, and the segment length l as

$$s = \left(\frac{v}{2l^3}\right)^{1/5} N^{3/5} l \tag{2}$$

so the blob is described by setting $s = \xi(r)$ and $N = N_\xi(r)$. The constraint on the total number of segments

$$2pN = 4\pi \int_0^R \frac{N_\xi}{\xi^3} r^2 \, dr \tag{3}$$

then determines the micelle radius as

$$R = \left(\frac{125}{18\pi}\right)^{1/5} p^{1/5} s = 1.172 p^{1/5} s \tag{4}$$

In the Daoud−Cotton model, all half-chains end exactly at $r = R$, where the area per chain midpoint is $\xi^2(R)$ with

$$\xi(R) = \xi_o = \left(\frac{125}{9}\right)^{1/5} (2\pi)^{3/10} p^{-3/10} s = 2.938 p^{-3/10} s \tag{5}$$

Alternatively, Li and Witten[19] relax this constraint on the midpoints and assume parabolic distributions for them and the segment densities, similar to those for planar brushes.[16] By minimizing the free energy with respect to the free end distribution and stretching of the polymers, they obtain the equilibrium brush height for polymers grafted to a sphere. Letting the radius of the spherical core vanish then yields the radius of a star or flowerlike micelle,

$$R = 1.206 p^{1/5} s \tag{6}$$

Since all ends lie within $r_c = 0.938R \le r \le R$, the outermost blob still satisfies eq 1 for reasonable p, so that

$$\xi_o = 3.023 p^{-3/10} s \tag{7}$$

Close to the edge, the chains are less stretched, and the ends (or midpoints in our case) are distributed as

$$\rho(r) = 1.01 \frac{p}{R^3}\left(5\frac{r^2}{R^2} - 2\right) \tag{8}$$

for $R > r > r_c$ and $\rho(r) = 0$ for $r < r_c$. When $6 > p > 1600$, $\xi_o > R - r_c$, indicating that all chain ends are located within the outermost blob. Distributing the ends lowers the free energy slightly and results in a radius (eq 6) and blob size (eq 7) with the same dependence on p but with somewhat larger prefactors than suggested by the Daoud−Cotton model, eqs 4 and 5.

Both the Daoud−Cotton and Li−Witten models predict the thermodynamic radius R of the micelle, whereas dynamic light scattering and viscometry detect the hydrodynamic radius R_H. To relate these two radii, we invoke the porous sphere model[20] to express the ratio R_H/R as a function of a hydrodynamic screening length λ,

$$\frac{R_H}{R} = \frac{1 + \Lambda \tanh(1/\Lambda)}{\frac{3}{2}\Lambda^2 + 1 + \Lambda \tanh(1/\Lambda)\left(\frac{11}{2}\Lambda^2 + 2\right)}$$

$$\approx 1 - \Lambda + \frac{1}{2}\Lambda^2 - 5\Lambda^3 + \ldots \quad \text{for } \Lambda \ll 1 \qquad (9)$$

with $\Lambda = \lambda/R$. For spherical micelles the segment density at the edge, i.e., in the outermost blob, must dominate λ. Therefore, $\lambda = \alpha\xi_o$, with α a proportionality constant dependent on the hydrodynamics within a single blob, which should be equivalent to a single coil with hydrodynamic size λ and root-mean-square end-to-end distance $s = \xi_o$. For a linear, flexible chain, the ratio of this hydrodynamic radius to the radius of gyration, $\lambda/r_g = 0.79 \pm 0.04$, is universal for all polymers and solvents.[21,22] Assuming the ratio $r_g/s = 1/6^{1/2}$ for a Gaussian coil determines α as

$$\alpha = \frac{\lambda}{s} = \frac{\lambda}{r_g}\frac{r_g}{s} = 0.32 \qquad (10)$$

allowing us to evaluate R_H/R from eq 14 with $R/\lambda \approx 3R/\xi_o$.

2.2. Associated Micelles. While two star polymers or diblock micelles in a good solvent always repel each other, bridging between triblock micelles generates an entropic attraction. This exchange of end blocks[14,15] doubles the configurations available to the hydrophobes and, thereby, reduces the free energy for flat plates by roughly 1 kT per chain in the area of contact. For spherical micelles that overlap by $\xi_o/2$, the overlap area (Figure 2) of $\pi\xi_o R$ divided by the area per blob ξ_o^2 provides an estimate of the attraction

$$-\frac{\Phi_{min}}{kT} = \pi\frac{R}{\xi_o} = 1.253p^{1/2} \qquad (11)$$

with the explicit dependence on $p^{1/2}$ following from eq 1 of the Daoud−Cotton model.

In the Li−Witten model, integration of the chain end density from eq 8 over this overlap region with $0 < \theta < \cos^{-1}(1 - \xi_o/(2R))$ (Figure 2b) and $\rho(r)$ for $R - \xi_o < r_c$ yields

$$-\frac{\Phi_{min}}{kT} = 1.011\pi p\frac{\xi_o}{R}\left(\frac{1}{3} - \left(\frac{r_c}{R}\right)^5 + \frac{2}{3}\left(\frac{r_c}{R}\right)^3\right) = 1.253p^{1/2} \qquad (12)$$

as well, showing the two to be numerically equivalent.

The estimate of Semenov et al. for the second virial coefficient corresponds to that for a hard sphere with radius R_{hs} and an attractive square well of depth Φ_{min} and width $\xi_o \ll R$, i.e.

$$A_2 \cong \frac{4\pi R_{hs}^3}{3}\left\{4 - 6\frac{\xi_o}{R_{hs}}\left[\exp\left(-\frac{\Phi_{min}}{kT}\right) - 1\right]\right\} \qquad (13)$$

The equivalent statistical mechanical model is the adhesive hard-sphere potential of Baxter,[23] characterized by the stickiness parameter $1/\tau$ which comprises the attractive component of the second virial coefficient, i.e.

$$\frac{1}{\tau} = 6\frac{\epsilon_0}{R_{hs}}\left[\exp\left(-\frac{\Phi_{min}}{kT}\right) - 1\right] \qquad (14)$$

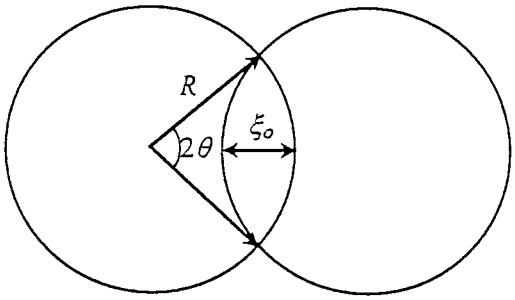

Figure 2. Schematic for associating spherical micelles with overlap width ξ_o and $\cos\theta = (R - \xi_o/2)/R$.

The simplicity of this model permits quantitative calculations of the binodal associated with the gas−liquid transition and the effect of pair interactions on the diffusion coefficient and the low shear viscosity in the dilute limit,[24]

$$\frac{D}{D_0} = 1 + (1.45 - 1.12/\tau)\phi \qquad (15)$$

$$\frac{\eta_0}{\mu} = 1 + 2.5\phi + (6.0 + 1.9/\tau)\phi^2 \qquad (16)$$

where ϕ is the volume fraction based on $R_{hs} = R_H$. Thus, macroscopic measurements allow one to deduce the strength of the attraction, since both the viscosity and diffusivity vary linearly with $1/\tau$ and, therefore, exponentially with the strength of the attraction. Of course, the potential and the hydrodynamic interactions are somewhat different than one would expect for flowerlike micelles, and as yet, no theory exists for the more concentrated solutions.

3. Experimental Details

3.1. Materials. Our associative polymers were synthesized at Rohm and Haas as linear poly(ethylene oxide) (PEO) homopolymer end-capped by C_{16} or C_{18} alkanes. For PEO with C_{16} hydrophobes, for example, a mixture of 150 g of PEO (35 kg/mol, Fluka Chemika) and 300 g of toluene were predried by azeotropic distillation. The mixture was cooled to 80 °C, and 2.1 g of hexadecyl isocyanate (Carbolabs Inc.) was added, followed by 0.2 g of dibutyltin dilaurate and then two additional shots of hexadecyl isocyanate (2.1 and 2.7 g, respectively). The reaction mixture was kept at 80 °C and monitored by IR until a distinct excess of isocyanate was observed. Hexanol (2 g) was then reacted with the excess isocyanate. After cooling to room temperature (~22 °C), the reaction mixture was dried under vacuum. The resulting polymer was purified by repeated recrystallization in tetrahydrofuran and hexane. A similar reaction yielded PEOs with the C_{18} end caps.

The molecular weight and purity of the unimers were thoroughly characterized, along with homopolymer PEO (Fluka Chemika) of the same molecular weight. Henceforth we will adopt the following nomenclature: ODU (octadecyl unimers) for PEO with C_{18} hydrophobes, HDU (hexadecyl unimers) for PEO with C_{16} hydrophobes, and PEO for the unmodified polymer. All have molecular weights close to 35 kg/mol.

Molecular weights and distributions were measured on a Perkin-Elmer HPLC equipped with a Waters 410 differential refractometer and two GPC columns (Progel TSK G3000 HXL and G4000 HXL) with THF as the elution solvent at 40 °C. Polystyrene served as the internal standard and monodisperse poly(ethylene oxides) (Polymer Laboratories) for calibration. A sample GPC graph is shown in Figure 3 for ODU. The results for ODU and HDU were $M_w = 34.2$ kg/mol ($M_w/M_n = 1.13$) and 35.3 kg/mol ($M_w/M_n = 1.10$), respectively. GPC does not differentiate the hydrophobic groups attached to the ends of the PEO chains and, therefore, sees the hydrophobically

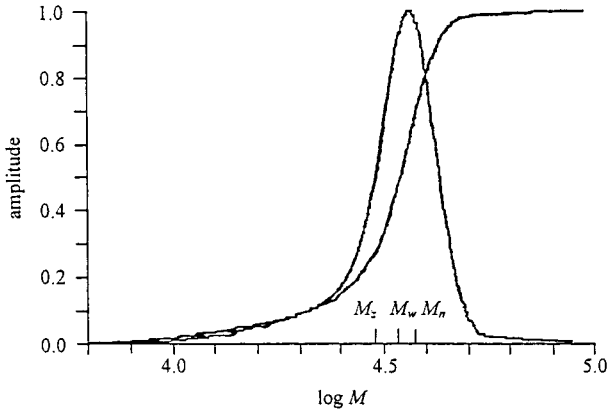

Figure 3. GPC spectrum for ODU with $M_w = 34.2$ kg/mol and $M_w/M_n = 1.13$.

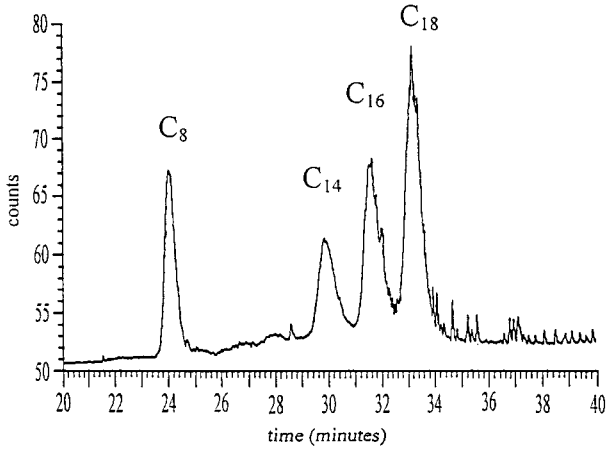

Figure 4. Reverse phase liquid chromatography spectrum of a mixture of 35 kg/mol unimers with hydrophobic end caps of various lengths.

modified and unmodified PEO as equal. The capping is apparent, however, from the Brookfield viscosities of 47.6 and 3.5 Pa s for 3 wt % aqueous solutions of ODU and HDU, respectively, compared to 0.003 Pa s for the unmodifed PEO.

To verify the hydrophobic modification, we employed reversed phase liquid chromatography (RPLC), a powerful technique for separating polymers according to their hydrophobicity. The analysis was performed with a Perkin-Elmer series 4 liquid chromatograph with an autosampler, a 200 μL loop injector, a Varex evaporative light scattering detector, and a Hamilton PRP-3 column (300A polystyrene−divinylbenzene). The solvent mixture varied continuously from 10/80/10 to 30/20/50 methanol/water/THF over 30 min, followed by an additional 10 min at the last concentration. The results (Figure 4) for a solution mixture of PEO chains (35 kg/mol) capped at both ends with identical alkyl groups (C_8, C_{14}, C_{16}, and C_{18}) indicate a clear separation with only small increments in the end group hydrophobicity. Individual samples of pure ODU or HDU display a single sharp peak on the RPLC spectrum (Figure 5) attesting to the uniformity of the hydrophobic modification (i.e., both ends fully capped).

A lower molecular weight analogue of ODU known as ODU-8 (C_{18} capped PEO of 8 kg/mol) was analyzed by MALDI/TOF, yielding a mass spectrum with a *z*-averaged molecular weight of $M_z = 9.69 \pm 0.05$ kg/mol, compared to the unmodified PEO with $M_z = 9.07 \pm 0.05$ kg/mol (Figure 6). The difference of 0.62 kg/mol reflects the two *n*-octadecyl isocyanate groups attached to the ends of the PEO.

Polymer solutions were prepared with doubly distilled deionized water containing 0−20 ppm hydroquinone as an oxidation inhibitor and stored at 4 °C, out of direct light, as further precaution against degradation. Dilute solutions for light scattering and capillary viscometry were prepared from

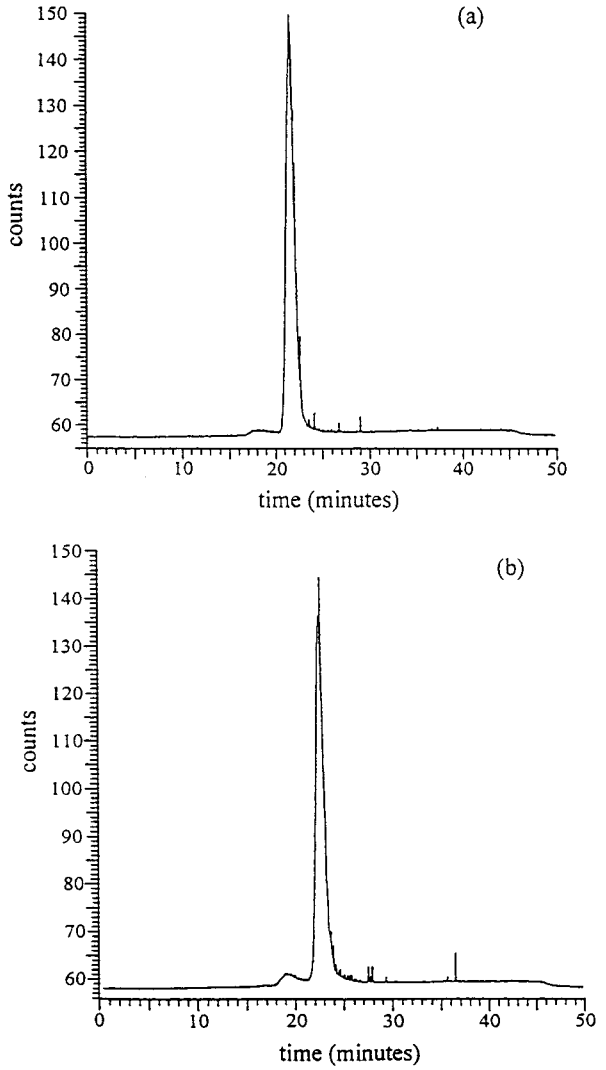

Figure 5. Reverse phase liquid chromatography spectra for purified (a) ODU and (b) HDU.

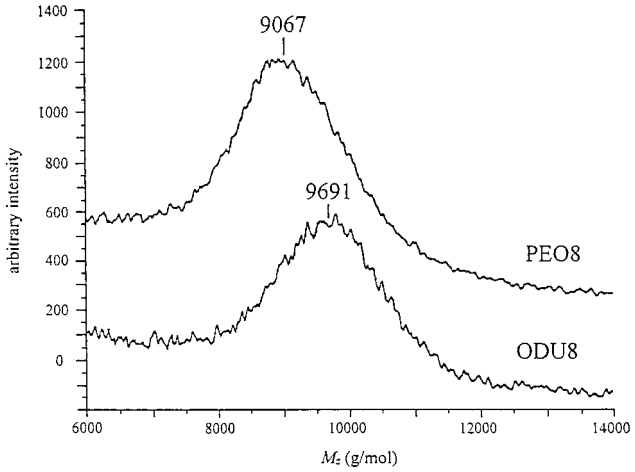

Figure 6. MALDI/TOF mass spectra of PEO (8 kg/mol) and the analogue end capped with C_{18} hydrophobes.

2 to 3 wt % stocks without the hydroquinone. The associative polymer was allowed to hydrate with periodic shaking over a week to achieve full solubilization and equilibrated at 25 °C before any measurement.

3.2. Methods. Polymer solutions between 0.25 and 2.5 wt % were thoroughly mixed and equilibrated at 25 °C over several months. Phase separation was monitored by detecting

the interface heights to ±0.05 mm as functions of time with a cathetometer and calculating the phase fractions as the height of the lower (condensed) or upper (dilute) phase relative to the total height. Once the fractions reached constant values, the upper, low-viscosity phase was decanted, and its polymer content was quantified with the Baleux assay,[25] which complexes the ethylene oxide units with iodine ions from a potassium iodide and iodine reagent. The concentration was determined colorimetrically via absorbance at 500 nm (Shimadzu UV1201 and Beckman DU-64 spectrophotometers) after calibration with associative polymer and PEO solutions of less than 20 ppm, where absorbance varies linearly with concentration. Multiple dilutions to bring solutions within this concentration range generated the dominant experimental uncertainties of 5−10%.

Light scattered by Brownian particles gives rise to intensity fluctuations that are generally quantified by an autocorrelation function that decays with time at a rate that depends on scattering angle θ. Photon correlation spectroscopy with a Lexel argon ion laser and a Brookhaven Instruments goniometer and correlator (BI-2030) was performed at $\theta = 90°$ and $\lambda = 514.5$ nm. Filtration through a hydrophilic membrane of 0.6−2 μm pores (Costar Nuclepore) removed dust with negligible change in the polymer concentration. For spherical scatterers, the first cumulant of the autocorrelation function yields the wavenumber and concentration-dependent diffusion coefficient $D(q,\phi)$. Equating the limit of D at infinite dilution to the Stokes−Einstein diffusion, $D_0 = kT/6\pi\mu R_H$, determines the effective hydrodynamic radius R_H of the particle, while the first-order correction characterizes the effect of pair interactions. Typically $qR_H = 0.39-0.46$ for ODU and HDU with wavenumber $q = (4\pi n_0/\lambda)\sin(\theta/2)$ and solvent refractive index n_0. Though not fully in the $qR_H \rightarrow 0$ limit, the measured D should be close to the mutual diffusion coefficient (eq 15).[24]

The kinematic viscosities of dilute polymer solutions were measured with Ubbelohde viscometers submerged in a temperature-controlled water bath at 25 ± 0.1 °C at conditions that minimize the Hagenbach−Couette kinetic energy correction. Normalizing the efflux times with those for the pure solvent generates reduced viscosities that vary with concentration c according to the Huggins equation

$$\frac{\eta - \mu}{\mu c} = \frac{t - t_0}{ct_0} = [\eta] + k_h[\eta]^2 c \qquad (17)$$

where t_0 is the solvent efflux time. Extrapolating to zero concentration determines the intrinsic viscosity $[\eta]$ from the intercept and the Huggins coefficient k_h from the slope. Solution densities measured with a Mettler/Paar DMA-45 densiometer deviate less than 0.1% from the value for water at 25 °C for $c < 1500$ ppm, eliminating any need to correct for the effect of polymer on the density.

4. Results

4.1. Phase Behavior. For our nearly monodisperse associative unimers, we find three distinct regimes beyond the critical micelle concentration ($c_{cmc} \sim 200$ ppm). The associative polymers form individual micelles in dilute aqueous solution and a highly associated solution at high concentrations. The transition between these two regimes is marked by a macroscopic phase separation. Solutions falling within the coexistence region separate into a low-viscosity dilute (upper) phase and a viscous condensed (lower) phase. We examined the phase boundaries characterizing the compositions of the coexisting phases as functions of total polymer concentration, temperature, hydrophobe size, and polymer molecular weight with copolymers consisting of C_{16} and C_{18} hydrophobes on 20, 27.5, and 35 kg/mol PEO and C_{14} hydrophobes on 20 kg/mol PEO.

As expected for a first-order phase transition, the fraction of the more concentrated phase increases linearly with total polymer concentration (Figure 7). Linear regression (extrapolation) indicates the lower and upper limits of the two-phase regime as 0.10 ± 0.03 and 1.77 ± 0.05 wt % for ODU and 0.24 ± 0.04 and 1.56 ± 0.07 wt % for HDU (Table 1). We confirmed the concentration of the isolated dilute phases directly via the colorimetric assay as approximately 0.2 wt % and the presence of micelles by photon correlation spectroscopy. From mass balances the concentration of the condensed phases follow at 2−3 wt %. Indeed these phases have low shear viscosities comparable to homogeneous micellar solutions prepared with 1.5−3 wt % polymer. These concentrations are less precise than, but consistent with, the extrapolated limits from Figure 7. The phase behavior is also reproducible; for example, upon dilution of the condensed phase with pure water back into the two-phase regime, the solution separates and reestablishes the expected equilibrium interface.

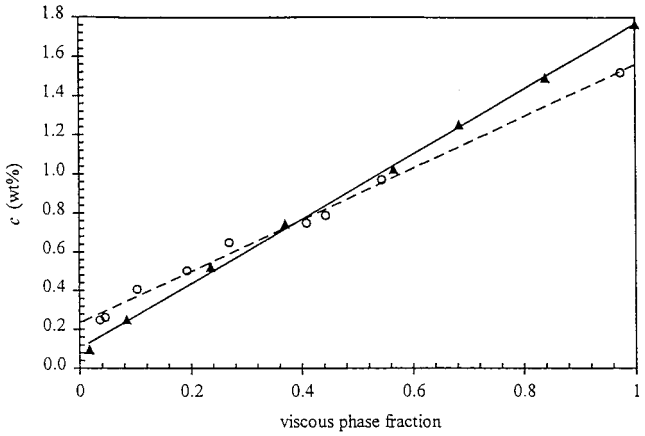

Figure 7. Fraction of lower, more concentrated, phase as a function of the total polymer concentration for ODU (▲) and HDU (○) with lines indicating linear least-squares fits.

Figure 8a−e shows the effect of temperature on the phase behavior for a variety of unimers with $M = 20-35$ kg/mol and $C_{14}-C_{18}$ hydrophobes. The two sets of concentrations in each plot delimit the two-phase regime. These data are less certain quantitatively than that in Figure 7 due to (1) extrapolation from a small number of samples over a limited range of concentrations and (2) possibly incomplete equilibration at each temperature. Despite some discrepancies between Figures 7 and 8a,b, the phase separation at 10−60 °C is clearly independent of temperature for C_{16} and C_{18} at the higher M_w (27.5 and 35 kg/mol), while showing some weak fluctuations (Figure 8d,e) for the 20 kg/mol unimers with $C_{14}-C_{16}$. These temperatures lie well below the lower critical solution temperatures of greater than 100 °C generally reported for PEO. Since PEO is generally soluble in water at all concentrations for these temperatures, e.g., with a Flory interaction parameter of 0.45 at 27 °C,[26] the phase separation observed with the unimers must be an entropically driven process related to the hydrophobic associations. Indeed, the less hydrophobic HDU solutions take longer to phase separate, especially near the upper phase boundary, and low in the coexistence region the phase separation sometimes disappears upon mixing and reequilibrating.

For hydrophobically modified linear PEOs, only occasionally has phase separation been reported. Glass et al.[27,28] did observe phase separation for completely capped telechelic associative polymers but reported the phenomenon to be elusive and inconsistent. Others note

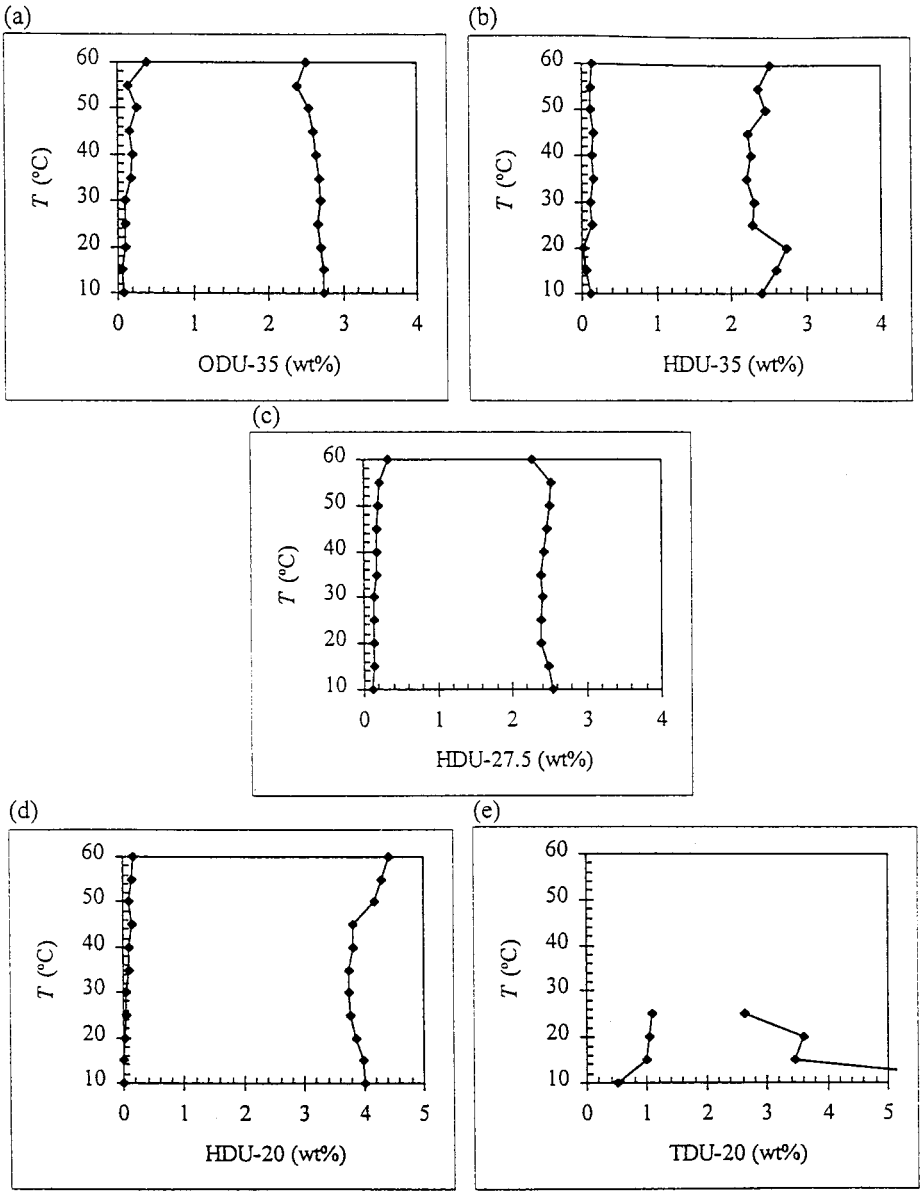

Figure 8. Phase boundaries as a function of temperature for (a) ODU (C_{18}-35 kg/mol), (b) HDU (C_{16}-35 kg/mol), (c) C_{16}-27 kg/mol, (d) C_{16}-20 kg/mol, and (e) C_{14}-20 kg/mol.

Table 1. Experimental Characterization of Triblock Micelles

	capillary viscosity			dynamic light scattering				phase behavior			
	$10^3[\eta]$, m^3/kg	k_h	$1/\tau$	$10^{12}D_0$, m^2/s	R_H, nm	$-k_d$	$1/\tau$	c_g/c_l, wt %	ϕ_g/ϕ_l	$1/\tau$	p
ODU	51 ± 0.5	13 ± 4	38 ± 12	10.3 ± 0.5	21.2 ± 1.3	7 ± 2	15 ± 4	0.10	0.02	13	33 ± 9
								1.77	0.36	12	
HDU	47 ± 3	15 ± 4	46 ± 13	12.9 ± 0.3	17.3 ± 0.4	4 ± 1	11 ± 2	0.24	0.04	11	20 ± 2
								1.56	0.29	11	
PEO	51 ± 1	0.3 ± 0.1									

that a viscous gel phase sometimes appears as the solid polymer is solvating but disappears upon agitation.[12] Francois et al.[29] reported macroscopic phase separation for linear associative polymers when the ratio of hydrophobe length to backbone length exceeded a critical value. For example, solutions of C_{12}-2, C_{12}-4, and C_{18}-20 (with the second number denoting molecular weight in kg/mol) separated into a dilute phase and an ordered "quasi-elastic" gel, but their C_{18}-35 did not phase separate. The temperature and concentration dependence of the phase behavior resembles our observations, though SAXS and SANS revealed the dense micellar phase for the smaller hydrophobes (C_{12}) to be ordered, in contrast to our disordered fluid phase.

Annable and Ettalaie[9] detected phase separation for mixtures of associative and unmodified PEOs of 35 kg/mol for mole fractions of the associative polymer less than 0.65 and total polymer concentrations exceeding 2 wt %. These associative polymers differ from ours in having the C_{16} hydrophobes linked by isophorone diisocyanates, a somewhat higher polydispersity (1.47), and an estimated 10−30% incompletely end-capped chains. Their coexisting phases had equal concentrations but quite different viscosities—one the high viscosity of an

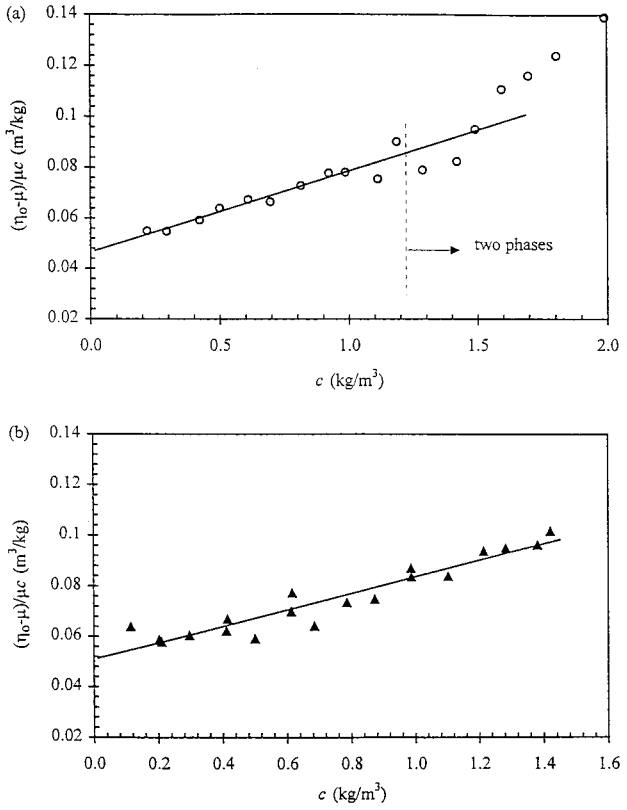

Figure 9. Reduced viscosities from capillary viscometry for (a) HDU (○) and (b) ODU (▲) with lines representing least-squares fits.

associated fluid and the other the low viscosity of a homopolymer solution.

Thus, only the observations of Glass seem to resemble ours, though his report is insufficiently detailed to draw a clear conclusion.

4.2. Micellar Solutions. When bridging between micelles is favorable, the micelles tend to form multiplets (or aggregates of multiple micelles), which produce the negative contribution to the second virial coefficient in eq 13. To compare our observations with the theories in section 2, we characterized the micellar structure to determine p and R_H directly and estimate Φ_{min} by deducing $1/\tau$ from measurable quantities with the assumption that $R_{hs} = R_H$.

Dilute, i.e., <2 kg/m^3 (or 2000 ppm), solutions of HDU and ODU were probed by capillary viscometry, light scattering, and fluorescence spectroscopy. The kinematic viscosities of the associative polymers (Figure 9) increase linearly at very dilute concentrations until the solution phase separates above 1.5 kg/m^3 or higher order interactions cause a general upturn. Fitting the linear portion of the data to the Huggins equation determines the intrinsic viscosity $[\eta]$ and the Huggins coefficient k_h (Table 1).

Values of $[\eta]$, describing the hydrodynamic volume per unit mass of solute, are slightly lower than reported for similar associative polymers by Jenkins et al.[30] (0.053 m^3/kg for H, 0.054 m^3/kg for C_{12}, and 0.067 m^3/kg for C_{16} at 30 °C). However, their synthesis, which links 8 kg/mol segments of PEO by isophorone diisocyanates to form the nominally 35 kg/mol backbone and adds end caps by coupling terminal groups (H, C_{12}, or C_{16}) via the same urethanes, results in a large polydispersity and 10−30% uncapped ends. These polymers and those of Annable et al.[9,12] described above will be designated

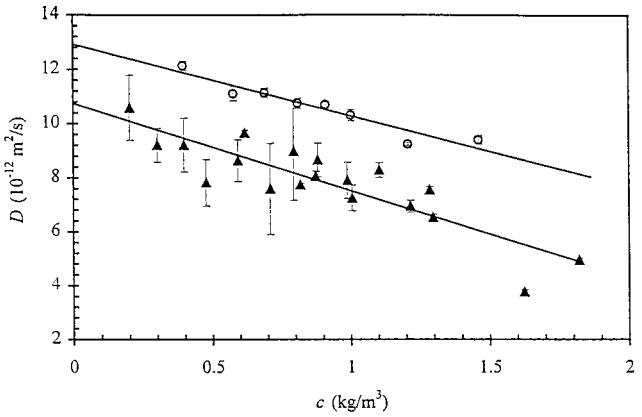

Figure 10. Diffusion coefficients as a function of polymer concentration for ODU (▲) and HDU (○) with solid lines indicating linear least-squares fits.

henceforth as C_n+IPDU. Comparison to unmodified PEO is debatable, since intrinsic viscosities reported in the literature vary from 0.029[31] to 0.048−0.058 m^3/kg[26,27,29] at 25 °C. Our PEO control yielded $[\eta] = 0.051 \pm 0.006$ m^3/kg, which is close to the values for the unimers.

The star polymer[17] and flowerlike micelle[14] models predict the volume per chain to decrease as $R^3/p \sim p^{-2/5}$ with increasing aggregation number. Though a decrease in permeability with increasing p moderates the trend, the roughly constant $[\eta]$ measured suggests that polymer chains may not be strongly stretched, as assumed in the theories.The Huggins coefficient, k_h, characterizing pair interactions in shear flow, is typically 0.4 for polymer in good solvent, 0.8 at Θ condition, and increases as the solvent quality decreases.[30,32] Jenkins et al.[30] reported $k_h = 0.35$ for H-terminated PEO and $k_h = 1-16$ for C_{12} and C_{16} end caps; the small k_h for H-terminated PEO supports their claim that internal urethane groups contribute negligibly to the hydrophobic interactions. Generally, they found k_h to decrease with increasing molecular weight, increasing temperature, and decreasing hydrophobe size. For our polymers, $k_h \sim 0.3$ for unmodified PEO signifies individual polymer coils in a good solvent, and $k_h = 12-15$ for the associative versions clearly arises from interactions between micelles.

Dynamic light scattering conducted for solutions above the critical micellar concentrations but in the one-phase regime measures the mutual diffusion coefficient (Figure 10)

$$\frac{D}{D_0} = 1 + k_d[\eta]c + \ldots \qquad (18)$$

Extrapolating to zero concentration estimates the diffusion coefficient of isolated micelles, $D_0 = (9.5 \pm 0.5) \times 10^{-12}$ m^2/s and $2R_H = 42.4 \pm 2.5$ nm for ODU and $D_0 = (12.9 \pm 0.3) \times 10^{-12}$ m^2/s and $2R_H = 34.5 \pm 0.8$ nm for HDU. The slopes produce the interaction coefficients, $k_d = -6.8 \pm 1.6$ for ODU and -4.3 ± 1.0 for HDU. The negative values indicate a strong attraction, which must also be responsible for the large Huggins coefficients.

For comparison, dynamic light scattering and pulse gradient NMR measurements at concentrations <1 wt %[4,7] have detected micelles with $D_0 = 1.2 \times 10^{-11}$ m^2/s for C_{16}+IPDU and 3.1×10^{-11} m^2/s for unmodified PEO (both 34 kg/mol), which correspond to $2R_H = 40.8$ and 15.8 nm, respectively. The self-diffusion coefficients from

Table 2. Aggregation Numbers for Associative Polymers

hydrophobe	M_w, kg/mol	$2p$	concn, wt %	method
C_{18} (ODU)	35	66 ± 18	<0.1	DLS and viscometry
C_{16} (HDU)	35	40 ± 4	<0.1	DLS and viscometry
		21 ± 1	0.4−1.2	fluorescence[33]
C_{16}+IPDU	34−50	20 ± 2	all	fluorescence[2,3,7]
	34	46 ± 2	dilute	DLS, viscometry, NMR[2,5,31]
C_{12}	21	28 ± 3	2−7	fluorescence[4]
C_{12}	13.5	80	2	DLS and viscometry[4,30]
		24	2	fluorescence[4]
C_{12}	9	34 ± 6	2.5	EPR[8]
pyrene	30	6 ± 1	0.02	fluorescence[35]

NMR studies generally decrease and develop a broader distribution as concentration and hydrophobe length increase, due to associations among the micelles. Since PEO chains of 35 kg/mol have ideal end-to-end distances of $s_0 = (2N)^{1/2}l = 11.4$ nm (with $2N = 628$, $l = 0.455$ nm[27]), water must act as a good solvent ($v/l^3 > 0.3$) in swelling the isolated coils to $s \sim 3R_H = 23.7$ nm. Crowding chains into the flowerlike micelles apparently drives a slightly more stretched configuration. Furthermore, chains stretch further as the hydrophobe size increases, because of the associated increase in aggregation number.

4.3. Aggregation Number. Equating the hydrodynamic specific volume indicated by the micellar radius extracted from dynamic light scattering, $4\pi R_H{}^3 N_A/3pM$, with the intrinsic viscosity permits an estimate of the aggregation number as

$$p = \frac{10\pi R_H{}^3 N_A}{3M[\eta]} \tag{19}$$

yielding $p = 33 \pm 9$ for ODU and 20 ± 2 for HDU. For C_{16}+IPDU (34 kg/mol), a combination of methods, DLS,[7] NMR,[5] and intrinsic viscosity,[31] yielded $p = 23 \pm 1$.

Unfortunately, values for the aggregation number seem to vary with method of measurement with fluorescence techniques generally giving smaller values. For example, Winnik and Yekta[33] monitored the fluorescence decay and extracted $2p = 21 \pm 1$ for our HDU, roughly half our value from intrinsic viscosity and dynamic light scattering. A similar discrepancy is observed for C_{16}+IPDU and other hydrophobe sizes (Table 2). Moreover, inference from a fluorescence study with pyrenes as the hydrophobes[34] yields very small aggregation numbers of about 6−8. The comparison of aggregation numbers is further complicated by differing polydispersities, urethane couplings, and even the degree of end capping, rendering the wide range of p values difficult to resolve.

With more certainty, fluorescence studies detect no change in micellar size from dilute concentrations up to 7 wt %. This supports the notion that increasing the concentration above the c_{cmc} primarily increases the number of micelles at fixed p, much as for surfactants.

5. Discussion

The intrinsic viscosities for dilute micellar solutions of ODU and HDU are comparable to those of unmodified PEO of the same molecular weight. However, the low value of the Huggins coefficient for PEO indicates swollen polymer chains in good solvent, whereas the much larger coefficients for the associative polymers suggest strong interaction between the micelles. The negative slopes for the mutual diffusion coefficients as a function of concentration establish the strong interaction between the micelles to be attractive. In the following, we seek to demonstrate that each of these is consistent with existing understanding of the structure of and interactions between flowerlike micelles.

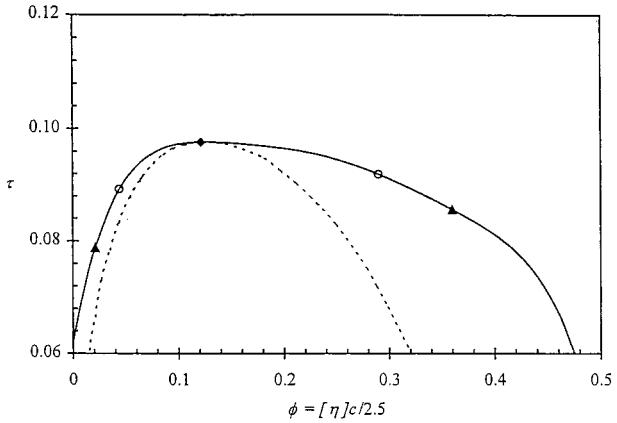

Figure 11. Adhesive hard-sphere phase diagram showing the binodal (—), the spinodal (- - -), and the critical point (◆) with the coexisting concentrations for ODU (▲) and HDU (○) superimposed onto the binodal.

To parametrize this interaction, we set aside for the moment the question of mechanism and model the associative micelles simply as adhesive hard spheres, i.e., with a short-range attraction and a hard-sphere excluded volume. With the volume fraction defined in terms of the hydrodynamic radius R_H such that $[\eta]c = 2.5\phi$, we have deduced values for the stickiness, $1/\tau$, from the concentration dependence of the diffusion coefficient, via eq 15, and the low shear viscosity, via eq 16. The stickiness or attraction from the diffusion data is larger for the longer hydrophobe ($1/\tau = 15 \pm 4$ and 11 ± 2 for ODU and HDU, respectively), whereas capillary viscometry yields much larger $1/\tau$ in both cases and a larger value for the shorter hydrophobe (Table 1). The reason for this difference between the two measurements is not hard to identify. In mutual diffusion, the associations play a passive role, solely setting the equilibrium microstructure. Furthermore, mutual diffusion does not drive relative motion of spheres in an interacting pair, making the process insensitive to flow in the gap between associated micelles. On the contrary, shear flow forces relative motion and thereby perturbs the microstructure from equilibrium. Furthermore, the dominant contribution to the Huggins coefficient is generated by the attractive force between the micelles and depends on the viscous stresses in the gap that retard motion. Thus, the adhesive hard-sphere model, which lacks any details of the micellar structure, could describe adequately the effect of pair interactions on mutual diffusion while failing miserably for the low shear viscosity. Hence, we turn to the phase behavior for another measure of the strength of the attraction. The adhesive hard-sphere model predicts a gas−liquid transition defined by binodal and spinodal curves with a critical point at $\phi_c = 0.1213$ and $\tau_c = 0.0976$ (Figure 11), though monodisperse adhesive hard spheres at $\tau < 0.13$ equilibrate as coexisting fluid and solid phases with the gas−liquid transition being metastable.[35] Our observation of an equilibrium gas−liquid transition for the micellar solutions suggests that polydispersity eliminates the slight advantage in free energy of the ordered phase and, hence, the fluid−solid transition. Superim-

Table 3. Comparison of Measurements with Calculations from Models with $N = 314$, $l = 0.454$ nm, and $v/l^3 = 0.31$

	HDU ($p = 20 \pm 2$, $s = 9.9$ nm)			ODU ($p = 33 \pm 9$, $s = 9.9$ nm)		
	expt	Daoud−Cotton	Li−Witten	expt	Daoud−Cotton	Li−Witten
R [nm]		21.1	21.7		23.3	24.0
ξ_o [nm]		11.8	12.2		10.2	10.5
R_H [nm]	17.3 ± 0.4	17.2	17.7	21.2 ± 1.3	20.0	20.6
$[\eta]$ [10^3m^3/kg]	47 ± 3	46	50	51 ± 5	44	48
Φ_{max}/kT		5.6/2.5	5.6		7.2/3.3	7.2
$1/\tau$	11 ± 2	1100/48	1100	15 ± 4	4100/83	4100

posing the volume fractions for the coexisting gas and liquid phases (on subsequent lines in Table 1) of ODU and HDU on the binodal curve of Figure 11 provides a purely thermodynamic estimate for the corresponding $1/\tau$ from the horizontal axis. As demonstrated in Table 1, the values are fully consistent with those deduced from the diffusion measurements.

Thus, the adhesive hard-sphere model enables us to quantify the effect of the attraction between micelles. For a mechanistic interpretation we now turn to Semenov et al.,[14] together with the Daoud−Cotton[17] and Li−Witten[19] models. For isolated triblock micelles, the radius is related to the blob size, the aggregation number, and the half chain molecular weight according to eq 4 or 6 as shown in Table 3. For triblocks of the same molecular weight, the micelle size increases with aggregation number, suggesting that the larger micelles consist of more highly stretched chains. The hydrodynamic radius R_H, calculated from eq 9 (Table 3) from both models, agrees remarkably well with our measured sizes for ODU and HDU, though the theories predict a more moderate p dependence than observed.

Moreover, rearranging eq 19 and incorporating R_H from eq 9 leads to

$$[\eta] = \frac{10\pi}{3}\frac{N_A}{Mp}R_H \tag{20}$$

which implies that $[\eta]$ should decrease with increasing p. Indeed, the $[\eta]$ calculated for ODU and HDU from the p determined by light scattering and viscometry (Table 3) vary inversely with p.

As for R_H, calculations from both models fall within experimental error of the measured values (Table 3). Since the measured values are equal within the experimental uncertainty, a dependence on p is not detectable.

As noted earlier, the attraction between associating micelles is expected to scale on the number of potential bridges, which Semenov et al. equated to the number of chain ends in the contact area $\pi\xi_o R$ between two spherical micelles residing in the attractive well. For the values of p detected the Daoud−Cotton and Li−Witten models are equivalent, since the latter predicts all ends to lie well within the outermost blob. Then from Figure 2b and eq 11 or 12, $-\Phi_{min}/kT = 5.6$ and 7.2 for HDU and ODU, respectively (Table 3), indicating that a similar number of bridges form as two micelles come into contact.

Assuming that $R_{hs} = R_H \gg \xi_o$ leads to estimates for the stickiness parameter $1/\tau$ (eq 16 and Table 3) that are much larger than determined experimentally (Table 2). Several simplifying assumptions could be at fault:

First, the attractive well is undoubtedly more parabolic than square, which replaces the $\exp(-\Phi_{min}/kT)$ with $(-\pi kT/4\Phi_{min})^{1/2}\exp(-\Phi_{min}/kT)$ and reduces $1/\tau$ by a factor of 2−3 over the range of interest.

Second, the width ξ_o of the attractive well is not small relative to the outer radius R of the micelle or the effective hard sphere radius R_{hs}. Accounting for this introduces a factor of $(1 + \xi_o/2R_{hs})$, which represents an $O(1)$ correction.

Third, the aggregation numbers are not terribly large, so the chains may not be sufficiently strongly stretched to conform to the approximations of either model. This might affect the distribution of ends more than the actual dimension of the layer. If, for example, one assumes the ends to be distributed uniformly over the outermost blob, rather than localized at the outer edge, the estimate of the attractive well drops to

$$-\frac{\Phi_{min}}{kT} = \frac{\pi R}{2\xi_o} - \frac{\pi}{12} \tag{21}$$

and yields about 2.5 for HDU and 3.3 for ODU. Then correcting for the shape and width of the well might produce values for $1/\tau$ similar to those observed.

Fourth, the entropy gain for the exchange of ends between two small micellar cores may fall off rapidly with lateral position for triblocks with midsegments off the centerline. This would reduced the effective number of bridges and could drop $1/\tau$ sharply below that estimated from the results for flat plates.

Overall, the concepts advanced by Semenov et al. and quantified through the Daoud−Cotton and Li−Witten models accord remarkably well with our measurements. The primary distinction is that Semenov et al. anticipated a fluid−solid transition, rather than the gas−liquid transition observed. Granted, our application of the theory involves estimates for the excluded-volume parameter v/l^3 and the hydrodynamic screening length ξ_H. In addition, the connection between micellar structure and the strength of the entropic attraction is a bit weak. A fully quantitative theory should treat the interactions between two micelles in more detail to account for the redistribution of chains upon compression and the actual configurations of bridging chains to obtain the interaction potential. Then more realistic thermodynamic and hydrodynamic models are needed to account for the considerable compressibility and permeability of the corona of the micelles.

6. Conclusions

Here we report the first quantitative observations of a gas−liquid transition between flowerlike micelles of associative triblock copolymers and offer detailed characterization of the micelles in dilute to moderately concentrated solutions. The behavior thereby observed is interpreted with the aid of several approximate models from the literature. First, the flowerlike associative micelles are treated as adhesive hard spheres to obtains sizes and interaction strengths that depend on hydrophobe size and aggregation number. Second, the Daoud−Cotton and Li−Witten models for micelles in a good solvent are invoked to confirm the relationships observed between micelle size and the aggregation

number. Third, the strength of the entropic bridging interaction between micelles deduced from the measurements is compared to expectations of Semenov et al. of 1 kT per chain in the overlap region. In a future paper we report the rheology of the associated condensed phases and its dependence on the structure of the micelles.

Acknowledgment. We thank the Rohm and Haas scientists**,** Robert E. Murphy and Paul O. Danis, for the reversed phase LC and MALDI/TOF analyses, respectively; Peter R. Sperry for sustained encouragement and advice in this undertaking; and Mitch Winnik and Ahmed Yekta for discussions of fluorescent measurements. We acknowledge financial support from the program in Particulate and Hydraulic Processes in the Division of Engineering of the National Science Foundation.

References and Notes

(1) Schaller, E.; Sperry, P. R. *Handb. Coat. Addit.* **1992,** *2*, 105−63.
(2) Winnik, M. A.; Yekta, A. *Curr. Opin. Colloid Interface Sci.* **1997**, *2*, 424−436.
(3) Wang, Y.; Winnik, M. A. *Langmuir* **1990**, *6*, 1437−1439.
(4) Alami, E.; Almgren, M.; Brown, W.; Francois, J. *Macromolecules* **1996**, *29*, 2229−2243.
(5) Macdonald, P. M.; Uemura, Y.; Dyke, L.; Zhu, X. *Adv. Chem. Ser.* **1996**, *248*, 377−393.
(6) Maechling-Strasser, C.; Clouet, F.; Francois, J. *Polymer* **1992**, *33*, 1021−1025.
(7) Yekta, A.; Xu, B.; Duhamel, J.; Adiwidjaja, H.; Winnik, M. A. *Macromolecules* **1995**, *28*, 956−966.
(8) Walderhaug, H.; Hansen, F. K.; Abrahmsen, S.; Persson, K.; Stilbs, P. *J. Phys. Chem.* **1993**, *97*, 8336−8342.
(9) Annable, T.; Ettalaie, R. *Macromolecules* **1994**, *27*, 5616−5622.
(10) Green, M. S.; Tobolsky, A. V. *J. Chem. Phys.* **1946**, *14*, 80−92.
(11) Tanaka, F.; Edwards, S. F. *J. Non-Newtonian Fluid Mech.* **1992**, *43*, 247−309.
(12) Annable, T.; Buscall, R.; Ettalaie, R.; Whittlestone, D. *J. Rheol.* **1993**, *37*, 695−726.
(13) Jenkins, R. D. Ph.D. Thesis, Lehigh University, 1990.
(14) Semenov, A. N.; Joanny, J.-F.; Khokhlov, A. R. *Macromolecules* **1995**, *28*, 1066−1075.
(15) Milner, S. T.; Witten, T. A. *Macromolecules* **1992**, *25*, 5495−5503.
(16) Milner, S. T.; Witten, T. A.; Cates, M. E. *Macromolecules* **1998**, *21*, 2610−2619.
(17) Daoud, M.; Cotton, J. P. *J. Phys. (Paris)* **1982**, *43*, 531−538.
(18) Flory, P. J. *Principles of Polymer Chemistry;* Cornell University Press: Ithaca, NY, 1953.
(19) Li, H.; Witten, T. A. *Macromolecules* **1994**, *27*, 449−457.
(20) Reuland, P.; Felderhof, B. U.; Jones, R. B. *Physica* **1978**, *93A*, 465−475.
(21) Schmidt, M.; Burchard, W. *Macromolecules* **1981**, *14*, 210−211.
(22) Wiltzius, P. *Phys. Rev. Lett.* **1987**, *58*, 710−713.
(23) Baxter, R. J. *J. Chem. Phys.* **1968**, *49*, 2770−2774.
(24) Russel, W. B.; Saville, D. A.; Schowalter, W. R. *Colloidal Dispersions;* Cambridge University Press: Cambridge, England, 1989.
(25) Baleux, B. *C. R. Acad. Sci. Ser. C* **1972**, *279*, 1617−1620.
(26) Brandrup, J.; Immergut, E. H. *Polymer Handbook*, 3rd ed.; Wiley: New York, 1989.
(27) Ma, Z.; Lundberg, D. J.; Roberts, S.; Glass, J. E. *J. Appl. Polym. Sci.* **1993**, *49*, 1509−1527.
(28) Kaczmarski, J. P.; Glass, J. E. *Macromolecules* **1993**, *26*, 5149−5156.
(29) François, J.; Maitre, S.; Rawiso, M.; Sarazin, D.; Beinert, G.; Isel, F. *Colloids Surf. A* **1996**, *112*, 251−265.
(30) Jenkins, R. D.; Bassett, D. R.; Silebi, C. A.; El-Aasser, M. S. *J. Appl. Polym. Sci.* **1995**, *58*, 209−230.
(31) Kato, T.; Nakamura, K.; Kawaguchi, M.; Takahashi, A. *Polym. J.* **1981**, *13*, 1037−1043.
(32) Gandhi, K. S.; Williams, M. C. *J. Polym. Sci. C* **1971**, *35*, 211−234.
(33) Winnik, M. A.; Yekta, A., private communication.
(34) Richey, B.; Kirk, A. B.; Eisenhart, E. K.; Fitzwater, S.; Hook, J. *J. Coat. Technol.* **1991**, *63*, 31−40.
(35) Rosenbaum, D.; Zamora, P. C.; Zukoski, C. F. *Phys. Rev. Lett.* **1996**, *76*, 150−153.

MA982007V